PHYSICAL REVIEW B VOLUME 28, NUMBER 5 1 SEPTEMBER 1983

Kinetics of ordering in two dimensions. I. Model systems

S. A. Safran, Paramdeep S. Sahni, and Gary S. Grest
Corporate Research Science Laboratories, Exxon Research and Engineering Company, P.O. Box 45, Linden, New Jersey 07036
(Received 22 March 1983)

The approach to equilibrium of ordered superlattice structures on surfaces is analyzed. Both Monte Carlo methods as well as analytic models of interacting domain walls are used to study the kinetics of quenched, two-dimensional systems with Q degenerate equilibrium states. In particular, the growth of long-range order in the magnetic analogs (Q-component Potts models) of the commensurate superlattice structures found on surfaces is analyzed in a study of the kinetics of typical domain geometries that are found when systems are quenched from high (disordered state) to low temperatures. Calculations and simulations of the time and temperature dependence of the domain sizes for the model system of isolated domains indicate that for two dimensions roughening fluctuations of the domain walls strongly influence the grain growth kinetics. Strip-shaped domains approach equilibrium almost entirely through these fluctuations, while circular domains shrink due to deterministic curvature, but with a rate that is strongly temperature dependent even for temperatures outside the critical region. Pinning effects in systems with $Q \geq 3$ lead to extremely slow kinetics for particular domain geometries. Low-temperature quenches on a triangular lattice indicate that these pinned geometries are rarely nucleated, while quenches on a square lattice equilibrate much more slowly due to pinning. The application of the theory to superlattice grain growth on surfaces is discussed in the following paper which presents results for the kinetics of quenched systems in terms of the simple domain geometries examined here.

I. INTRODUCTION

Recent experimental interest has focused on the lattice structures observed for atoms that are adsorbed on solid surfaces.[1] At high temperatures, the adsorbed atoms are in a disordered (gas or liquid) phase on the surface while at low temperatures, they form periodic structures. If the surface density of adsorbed atoms is less than the surface density of substrate atoms, the periodic structures formed have lattice constants that are larger than the substrate lattice constants and are known as superlattices. For physisorbed systems, such as rare-gas atoms adsorbed on graphite, superlattices that are either commensurate[2] (i.e., the superlattice periodicity is an integral multiple of the substrate lattice constant) or incommensurate[3] with the substrate periodicity have been observed. On the other hand, the stronger interactions that exist in chemisorbed systems [e.g., O/W(110),[4] O/Ni(111),[5] H/W(001) (Ref. 6)] usually result in a commensurate overlayer of atoms. In addition to surface studies, similar superlattice structures have also been observed in intercalation compounds,[7] where the large spacings between intercalant layers can result in quasi-two-dimensional behavior.

Although most experimental and theoretical studies have centered on the equilibrium properties and phase transitions of surface superlattice structures, some aspects of the kinetics have been examined as well. Experimental studies[4] of oxygen atoms on tungsten [O/W(110)] have reported a slow evolution of the domains of an ordered superlattice. Monte Carlo simulations of adsorbed atoms on surfaces quenched from high to low temperatures ($T < T_c$) have also found very long equilibration times resulting in disordered, quenched-in polycrystalline structures.[8–11] Lifshitz[12] was the first to predict slow kinetics in magnetic systems with several degenerate equilibrium states. Recently, Lifshitz's arguments were extended[13] to show how the competition between various types of domain walls between regions with thermodynamically degenerate superlattices which differ only by their orientation, can result in the polycrystalline structures observed in the simulations performed in Refs. 8–11.

In this paper and in the following one,[14] we present a detailed theoretical study of the time and temperature dependence of domain sizes for ordering systems with several degenerate equilibrium states. The system is quenched from a high-temperature disordered state to low temperatures below the critical temperature T_c, and the kinetics of ordering are analyzed. We show that the approach to equilibrium is influenced by the effects of roughening fluctuations,[15] domain-wall interactions, and pinning in two dimensions. These effects result in both quantitative as well as qualitative modifications of the usual theory of domain growth developed for three-dimensional systems.[12,16,17] In two dimensions, domain growth rates become strongly temperature dependent, while domain-wall competition can result in a disordered structure characterized by the quenched-in domains of some average size. In addition to the theoretical interest, an understanding of the kinetics of ordering is important from a practical viewpoint, since the chemical and elastic properties of epitaxial layers are functions of the domain sizes. For ordering alloys in three dimensions, both theoretical and experimental studies of domain kinetics are well known in both the physics and the metallurgical literature.[12,16,18] It is the extension of these theories to two-dimensional superlattice ordering that is the purpose of the present work, which we hope will provide an impetus for experimental measurements of the kinetics of or-

dering on surfaces. In this paper simple domain geometries are studied using both an analytic domain-wall model as well as Monte Carlo simulations. In the following paper the results of global quenches of large systems are presented. The kinetics of the quenched systems is related to the kinetics of the model domain geometries discussed in this paper. Preliminary versions of some of the material in this paper were presented in Refs. 13 and 19–22.

The organization of this paper is as follows. In Sec. II we introduce the magnetic analogs of the superlattice structures. The present analysis is couched in the language of magnetic ordering, and is limited to a simplified description of surface superlattices. In this section we also introduce the analytic domain-wall model and the Monte Carlo method used in our calculations. In Sec. III we present the results of our calculations and simulations for isolated domains in two-component systems. We show how the roughening of the domain walls by thermal fluctuations results in a strong temperature dependence for the kinetics of circular domains and in a relatively quick equilibration for strip-shaped domains. These results are in contrast to the situation in three dimensions,[17] where circular domains have a growth-shrinking rate that is not intrinsically temperature dependent and where infinite strip domains are strongly metastable. We report the analysis of multicomponent (degeneracy $Q \geq 3$) systems in Sec. IV where we treat the kinetics of simple domain geometries. The specific domain-wall geometries that lead to frozen-in or blocked structures are identified and the annealing of these structures at high temperatures is demonstrated. The relevance of these model systems to the equilibration of large quenched systems is discussed in the following paper where we present the results of Monte Carlo simulations of quenches from high to low temperatures.

II. THEORETICAL KINETIC MODELS

In this section, we relate the lattice-gas representation of adsorbed atoms and commensurate superlattices to the magnetic models used in our calculations. We present the kinetic equations governing the equilibration of these magnetic models as used in the Monte Carlo simulations. Finally, we derive the equations of motion for interacting, fluctuating, domain walls that are used in our analytic calculations which make use of a continuum approximation.

A. Adatom: spin models and Monte Carlo procedure

Commensurate overlayers of atoms on surfaces have been commonly described by lattice-gas models with interactions which extend to several neighbors.[23] The substrate defines a regular array of preferred adsorption sites and each adsorption site can be either empty or occupied by a single adatom. For atoms whose effective sizes (e.g., the Lennard-Jones diameter) are larger than the lattice size of the substrate, the maximum ratio of adsorbed atoms to substrate sites is less than unity. As an example, consider the adsorption of krypton (Lennard-Jones diameter 3.60 Å) on the hexagonal basal plane of graphite (see Fig. 1) where the nearest-neighbor separation of adsorption sites is 2.46 Å, resulting in a nearest-neighbor exclusion as

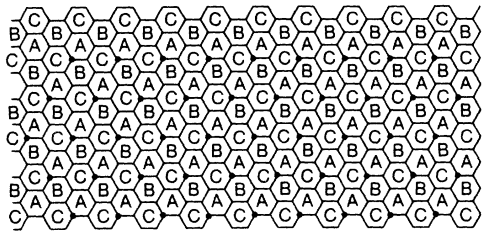

FIG. 1. Sublattice sites labeled A, B, and C for the $\sqrt{3}\times\sqrt{3}$ structure applicable to adsorption on the hexagonal basal plane of graphite. The dots label the sites of the "Potts lattice," each site of which includes an A, B, and C site of the original lattice.

described above. Further neighbor interactions are attractive and short ranged. For a commensurate overlayer, the maximum ratio of krypton atoms to graphite sites is $\frac{1}{3}$ and there are three possible triangular superlattice arrangements which differ from each other by only unit translations.

The important feature of the superlattice ordering for Kr/graphite is the existence of three possible equilibrium states which are degenerate in their (free) energy. The entire lattice can be subdivided into sites belonging to one of these three possible superlattices. At high temperatures, for coverages of less than $\frac{1}{3}$, the occupation of any one of these superlattices is random, while for low temperatures, only one of the three possible sublattices is occupied, resulting in a structure with long-range order. For a coverage of exactly $\frac{1}{3}$, a random occupation is, of course, impossible if the constraint of nearest-neighbor exclusion is maintained. However, the introduction of vacancies and/or imperfect registry can relax this constraint. In the present work, the presence of vacancies and/or incommensurately adsorbed atoms is not explicitly taken into account. Implicitly, however, these effects are presumed to be responsible for the finite energy of domain-wall boundaries between regions of different superlattice (see Fig. 2), where the constraint of nearest-neighbor exclusion has been relaxed. We thus consider the case of maximum coverage ($\frac{1}{3}$ in the previous example) and account for the canceling effects of nearest-neighbor exclusion and vacancies or discommensurations by allowing nearest-neighbor occupation of two different sublattices, but with a large but finite positive energy contribution. We note that not all superlattice structure can be mapped even approximately into simple Potts models. For example, O/W(110) orders in a superlattice with four degenerate ground

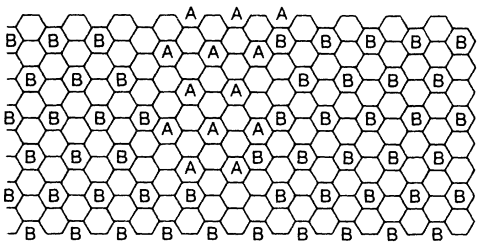

FIG. 2. Two neighboring domains of regions of ordering on sublattice A and sublattice B (see Fig. 1) result in domain walls where there is nearest-neighbor occupancy of A and B sites.

states.[4] However, the lattice is completely covered by only two of the four states and the system is not represented by a simple four-state Potts model.

To incorporate the constraint of constant coverage, we map the actual lattice gas into a Potts spin model.[24] This has been described for the case of krypton on graphite in Ref. 23. For the case of maximum coverage, in the approximation described above, each set of three adjacent A, B, and C sublattice sites in Fig. 1 are mapped into one site of triangular lattice (the Potts lattice), as shown in Fig. 1. At each lattice site, we place a Potts spin which can "point" in one of three possible directions, each direction corresponding to the occupation of either the A, B, or C site. The nearest-neighbor exclusion is taken into account by allowing only one of the sites to be occupied. However, the possibility of domain boundaries between two different sublattices (Fig. 2) still exists since two neighboring sites on the Potts lattice can have spins pointing in different directions, corresponding to the occupation of neighboring A and B or C sites. A more detailed mapping of the lattice-gas problem to the Potts model, which explicitly takes into account vacancies, was presented by Berker *et al.* in Ref. 23 where only the equilibrium properties of the overlayer were considered. The kinetics of the more realistic model will be analyzed in future reports.

Although the case of the threefold-degenerate superlattices appropriate to the $\sqrt{3}\times\sqrt{3}$ structure was explicitly described above, similar mappings of the adatom commensurate structure to Q-component ferromagnetic Potts models can be done for degeneracies $Q>2$. The nearest-neighbor repulsions are accounted for by the mapping to the Potts model and the longer-range attractive interactions are transformed into spin-spin interactions with the Hamiltonian,

$$H=-J\sum_{\langle ij\rangle}\delta_{S_iS_j}\ , \tag{1}$$

where $S=A,B,C,\ldots$ is one of the Q states and $\delta_{S_iS_j}$ is the Kronecker function. For simplicity, the sum is over nearest-neighbor spins on the Potts lattice and $J>0$. When $Q=2$, the Hamiltonian is equivalent to the Ising-model Hamiltonian. We note that for $Q=2$, the ferromagnetic Potts model on the Potts lattice is actually the result of a transformation of the antiferromagnetic Ising model appropriate to the real lattice-gas system with half of the sites filled (i.e., fixed total magnetization equal to zero). Using Monte Carlo techniques,[25] we have studied both model domain geometries with well-defined initial conditions (this paper) as well as systems which are quenched from the disordered state ($T\gg T_c$) to the ordered state ($T<T_c$) (following paper). We have analyzed the time and temperature dependence of the sizes of the ordered domains as the system approaches equilibrium. To reduce the effects of the boundary, in our studies of quenched systems, we have studied very large systems, up to 200×200 sites with periodic boundary conditions. For the study of the kinetics of single domains, the lattice size used was always much larger than the size of the domain of interest.

Dynamics for the spins are introduced in the standard manner[25] for both Glauber as well as Kawasaki dynamics. Since it is the sublattice ordering that is the focus of the present work, and the order parameter (sublattice occupation—magnetization) is a nonconserved variable,[26] Glauber dynamics are sufficient to describe the basic physical processes. However, for the study of systems where only two types of domains are important (see Sec. III), we have also simulated the Kawasaki dynamics of antiferromagnetically coupled Ising spins, which correspond to the actual sublattices (spin-up is occupied, spin-down is unoccupied). This allows a study of the more realistic processes relevant to surface adsorption where atoms change their sublattice occupation by hopping to empty sites—i.e., by an interchange of occupied (spin-up) and unoccupied (spin-down) sites. In the case of Glauber dynamics, we choose a site randomly and compute the change in energy ΔE to flip the spin at that site. We next obtain the transition probability W using

$$W=\begin{cases}\dfrac{1}{\tau}e^{-\Delta E/kT}, & \Delta E>0\\[2ex] \dfrac{1}{\tau}, & \Delta E\le 0\ ,\end{cases} \tag{2a}$$

where k is the Boltzmann constant and T is the temperature. The constant τ sets the time scale for the Monte Carlo study. Since $1/\tau$ is like an attempt frequency, we expect it to have an Arrhenius temperature dependence for any particular experimental system. Thus $\tau\propto\exp(-Q'/kT)$ where Q' is an activation energy related to the coupling to the heat bath. In the following calculations, τ just sets the (possibly temperature-dependent) time scale. However, if $Q'\ll kT$, τ is independent of temperature for the growth kinetics. In any case, the temperature dependence introduced by τ, although important in a detailed comparison of theory and experiment, is unrelated to the cooperative interactions between the spins. Using Eq. (1), the transition probability W is computed and compared to a random number R ($0\le R\le 1$) and the spin is changed if $W>R$; otherwise, the old configuration is retained. In the case of Kawasaki dynamics, the procedure is similar, except that we randomly choose nearest-neighbor pairs of spins for exchange. The energy ΔE is computed before and after the spins are exchanged. The transition probability W' is defined by

$$W'=\frac{1}{\tau}\frac{e^{-\Delta E/kT}}{1+e^{-\Delta E/kT}}\ . \tag{2b}$$

As above, the exchange is carried out only if $W'>R$. For both types of dynamics, the configurational averaging is obtained by averaging the data over many runs.

B. Domain-wall model

Although Monte Carlo methods have the advantage of being able to simulate a wide variety of domain-growth situations, additional physical insight into the mechanisms and dynamics of domain growth can be obtained from analytic studies of model systems.[27–29] In principle, it would be desirable to calculate the kinetics of a Potts model at all stages of the approach to equilibrium from a high-temperature quench. However, such global, analytic

calculations are first now being performed[29] for even the simple two-component Ising systems. Field-theory calculations have been performed for the "early" time regime, where well-defined domains are not yet present.[16,27] Other calculations, which have as their basis the kinetics of the domain walls (as opposed to the spins), have been reported for later times.[17,28] For example, Ref. 17 discusses the role of curvature energy in the kinetics of grain growth and shows that a spherical domain of one sublattice (spin-up) surrounded by an infinite sea of the other sublattice (spin-down) shrinks with its area decreasing linearly with time.

In the present work, we use a model of interacting, fluctuating domain walls to analyze the kinetics of particular domain geometries. When a given domain-wall geometry is specified, the stochastic equations of motion for the domain walls are derived from the standard equations of motion for the entire spin (or sublattice) system. Away from the intersections points of three or more domain walls, a given wall separates only two degenerate states (even for $Q>2$). Section IV contains a dicussion of the pinning effects of wall intersections. Here, we derive equations of motion for simple wall configurations which separate two degenerate domains. We thus consider only the ferromagnetic Ising model in a continuum approximation for both the spins and the lattice. Remembering that S represents the sublattice occupation which is a nonconserved order parameter, the Langevin equation of motion for $S(\vec{r},t)$ is[26]

$$\dot{S}=-\frac{\delta F}{\delta S}+\eta_S \ , \tag{3}$$

where $\dot{S}=\partial S/\partial \tilde{t}$. The dimensionless time $\tilde{t}=t/\tau$, where τ is the hopping time which may be temperature dependent. In Eq. (3), $F[S(\vec{r},t)]$ is the free-energy functional which is written for a nonhomogeneous spin distribution in the continuum approximation as

$$F=\int d\vec{r}\,[\tfrac{1}{2}J\,|\,\vec{\nabla}S(\vec{r},t)\,|^2+Jg(S(\vec{r},t))] \ , \tag{4}$$

where $g(S(\vec{r},t))$ is a nonlinear function of the order parameter. In Eq. (4), all lengths are scaled by the lattice constant. Near the domain wall, the order parameter is small so that g can be expanded as

$$g\simeq-\tfrac{1}{2}\alpha S^2+\tfrac{1}{4}\beta S^4 \ . \tag{5}$$

For $T<T_c$, both α and β are positive and $\alpha\propto(T_c-T)/T_c$ for T near T_c. In the Langevin equation of motion for $S(\vec{r},t)$, η_S is the stochastic noise which is assumed to be delta correlated in both space and time,[26]

$$\langle\eta_S(\vec{r},t)\eta_S(\vec{r}',t')\rangle=2kT\,\delta(\vec{r}-\vec{r}')\delta(\tilde{t}-\tilde{t}') \ , \tag{6a}$$

$$\langle\eta_S(\vec{r},t)\rangle=0 \ . \tag{6b}$$

Stationary solutions of Eq. (3) exist which consist of two domains separated by a wall at $x=0$, i.e., $S_0(\vec{r})$ is given by the solution of

$$\frac{\partial g}{\partial S}-\nabla^2 S=0 \tag{7}$$

with boundary conditions at $x=\pm\infty$ of $S_0(x)\rightarrow\pm S_e$

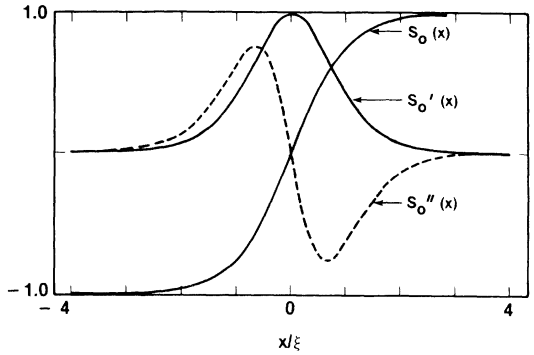

FIG. 3. One-dimensional, time-independent domain-wall solution to Eq. (7). The magnitude of the local spin field at position x normalized to the domain-wall width is shown, as are its first two derivatives.

where S_e is the two-dimensional equilibrium value obtained by setting

$$\left[\frac{\partial g}{\partial S}\right]_{S=S_e}=0 \ . \tag{8}$$

For a general $g(S)$ which has only two degenerate minima, the behavior of $S_0(\vec{r})$ and its derivatives is shown in Fig. 3. For $x\rightarrow\pm\infty$, $S_0(\vec{r})$ approaches $\pm S_e$ with only exponentially small corrections, while near $x=0$, there is a linear region where $S_0(\vec{r})$ changes sign in a region of width ξ. For example, for the form for $g(s)$ given in Eq. (5), there is a one-dimensional solution,[16]

$$S_0(x)=S_e\tanh\frac{2x}{\xi} \ , \tag{9}$$

where $\xi=(8/\alpha)^{1/2}$ is proportional to the two-dimensional correlation length. In the present work, the temperatures of interest are low enough so that critical fluctuations can be neglected. At very low temperatures, the domain-wall width approaches the lattice constant, which is set to unity in our calculations.

An effective stochastic equation for the motion of a domain wall can be derived from Eq. (3) by looking for a shape-invariant solution for the domain wall with the wall location $x=X_0(y,t)$ being a stochastic variable that is both time and space dependent. We thus write $S(\vec{r},t)=S_0[x-X_0(y,t)]$ and use the equation of motion for S_0 to find

$$-S_0'\dot{X}_0=JS_0''-JS_0'\frac{\partial^2 X_0}{\partial y^2}+JS_0''\left[\frac{\partial X_0}{\partial y}\right]^2-J\frac{\partial g}{\partial S}+\eta_S \tag{10}$$

with $S_0'=\partial S_0/\partial x$. For $x\simeq X_0(y,t)$, we approximate $S_0'(0)=2S_e/\xi$ and $S_0''(0)=0$ to find to lowest order in $\partial X_0/\partial y$,

$$\dot{X}_0=J\frac{\partial^2 X_0}{\partial y^2}+\eta \ . \tag{11}$$

In Eq. (11), η is proportional to the effective noise on the boundary, i.e.,

$$\eta=-\eta_S(x=X_0(y,t),y,t)\frac{\xi}{2S_e} \ .$$

Since we deal with lattice systems, the δ-function correlations for η_s [Eq. (6)] are appropriate only for large distances. At small distances (less than a correlation length), the correlations are unity. The correlation functions for η are

$$\langle \eta(y,t)\eta(y',t')\rangle = \frac{\xi^2}{2S_e^2} kT\,\delta(y-y')\delta(\tilde{t}-\tilde{t}') , \tag{12}$$

$$\langle \eta(y,t)\rangle = 0 . \tag{13}$$

Kawasaki and Ohta[28] have presented a more rigorous derivation of these equations and have shown that there exist corrections to Eq. (11) of order $(\partial X_0/\partial y)^2$. A similar procedure can be used to find the equation of motion of a circular domain wall. In polar coordinates, Eq. (3) becomes

$$\dot{S} = -J\frac{\partial g}{\partial S} + \frac{J}{r}\frac{\partial}{\partial r} r \frac{\partial S}{\partial r} + \frac{J}{r^2}\frac{\partial^2 S}{\partial \theta^2} + \eta_S . \tag{14}$$

We write $S(r,t)=S_0[r-R(\theta,t)]$ and use Eq. (14) to find

$$-S_0'\dot{R} = -J\frac{\partial g}{\partial S} + JS_0'' + \frac{J}{r^2}S_0''\left[\frac{\partial R}{\partial \theta}\right]^2 + S_0'\frac{J}{r} - \frac{J}{r^2}S_0'\frac{\partial^2 R}{\partial \theta^2} + \eta_S . \tag{15}$$

Again, for $r \simeq R(\theta,t)$, $S_0''(0)=0$, and to lowest order in $(\partial R/\partial\theta)$ we find the equation of motion

$$\dot{R} = \frac{-J}{R} + \frac{J}{R^2}\frac{\partial^2 R}{\partial \theta^2} + \frac{\eta}{R^{1/2}} \tag{16}$$

with noise correlations

$$\langle \eta(\theta,t)\eta(\theta',t')\rangle = \frac{\xi^2}{2S_e^2} kT\,\delta(\theta-\theta')\delta(\tilde{t}-\tilde{t}') . \tag{17}$$

The unusual form for the noise term is a consequence of the property of the δ function in polar coordinates.

Interactions between the domain walls are shown to be short ranged, due to the fact that $S_0(\vec{r})$ approaches its asymptotic value with only exponential corrections for $x \gg 0$ or $x \ll 0$. Again this approximation breaks down near the critical point, but is good for the region of interest in our calculations. We include interactions between the walls by writing a coupled set of equations of motion of, for the two walls at $x=h_1(y,t)$ and $x=h_2(y,t)$, respectively,

$$\dot{h}_1 = J\frac{\partial^2 h_1}{\partial y^2} - \frac{\partial}{\partial h_1}V(h_1-h_2) + \eta_1 , \tag{18a}$$

$$\dot{h}_2 = J\frac{\partial^2 h_2}{\partial y^2} - \frac{\partial}{\partial h_2}V(h_1-h_2) + \eta_2 , \tag{18b}$$

where η_1 and η_2 are the noises on the two walls. It is assumed that they are uncorrelated with each other. Their self-correlations are given by Eq. (13). In Eq. (18), the first term on the right-hand side is the curvature driving force which is the same as in the independent wall equations. The second term is the attractive force due to the interaction $V(h_1-h_2)$ between the walls. This interaction is attractive and short ranged, since it is only when the walls annihilate that the free energy is lowered. For large wall separations, $V(h_1-h_2)$ goes to zero exponentially, and the equations of motion for two independent walls are recovered.

A derivation of this equation for the case where $g(S)$ is given by Eq. (5) is obtained by writing S for two interacting walls[30,31]

$$S = S_e \tanh\left[\frac{2}{\xi}[x-h_1(y,t)]\right]\tanh\left[\frac{2}{\xi}[x-h_2(y,t)]\right] . \tag{19}$$

From the equation of motion for S we find that

$$\dot{S} = J\alpha S_e \operatorname{sech}^2 Z_1 \operatorname{sech}^2 Z_2 (1-\tanh Z_1 \tanh Z_2) + \eta_S \tag{20}$$

with

$$Z_i = \frac{2}{\xi}(x-h_i) .$$

Looking locally near $x=h_1(y,t)$ and $x=h_2(y,t)$ and keeping terms that are linear in the small quantity $e^{-|h_1-h_2|}$ as well as the time and space derivatives of h_1 and h_2, we recover Eqs. (18) as given above. We thus identify the interaction $V(h_1-h_2)$ with

$$V(h_1-h_2) = -4J\exp(-4|h_1-h_2|/\xi) . \tag{21}$$

More rigorous treatments can be found in Ref. 28. Finally, defining the relative wall separation $h=h_1(y,t)-h_2(y,t)$, we obtain the equation of motion

$$\dot{h} = J\frac{\partial^2 h}{\partial y^2} - 2\frac{\partial V(h)}{\partial h} + \eta_T , \tag{22}$$

where η_T is the total noise acting on $h(y,t)$ with correlations

$$\langle \eta_T(y,t)\eta_T(y',t')\rangle = 2\frac{\xi^2}{2S_e^2} kT\,\delta(y-y')\delta(\tilde{t}-\tilde{t}') . \tag{23}$$

At low temperatures $\xi, S_e \to 1$. We shall use this approximation in the following sections.

III. FLUCTUATION EFFECTS FOR ISOLATED DOMAINS

In this section, we calculate the kinetics of isolated domains, e.g., a single domain of spin up surrounded by an infinite sea of spin down. This simple configuration often dominates the late stage kinetics of three-dimensional metallurgical systems where fluctuation effects are generally unimportant. We show that the effects of thermal roughening fluctuations in two dimensions greatly speed up the kinetics of strip-shaped domains. For circular geometries, these fluctuations result in a strong temperature dependence of the growth-shrinking rate which can be measured in scattering experiments.

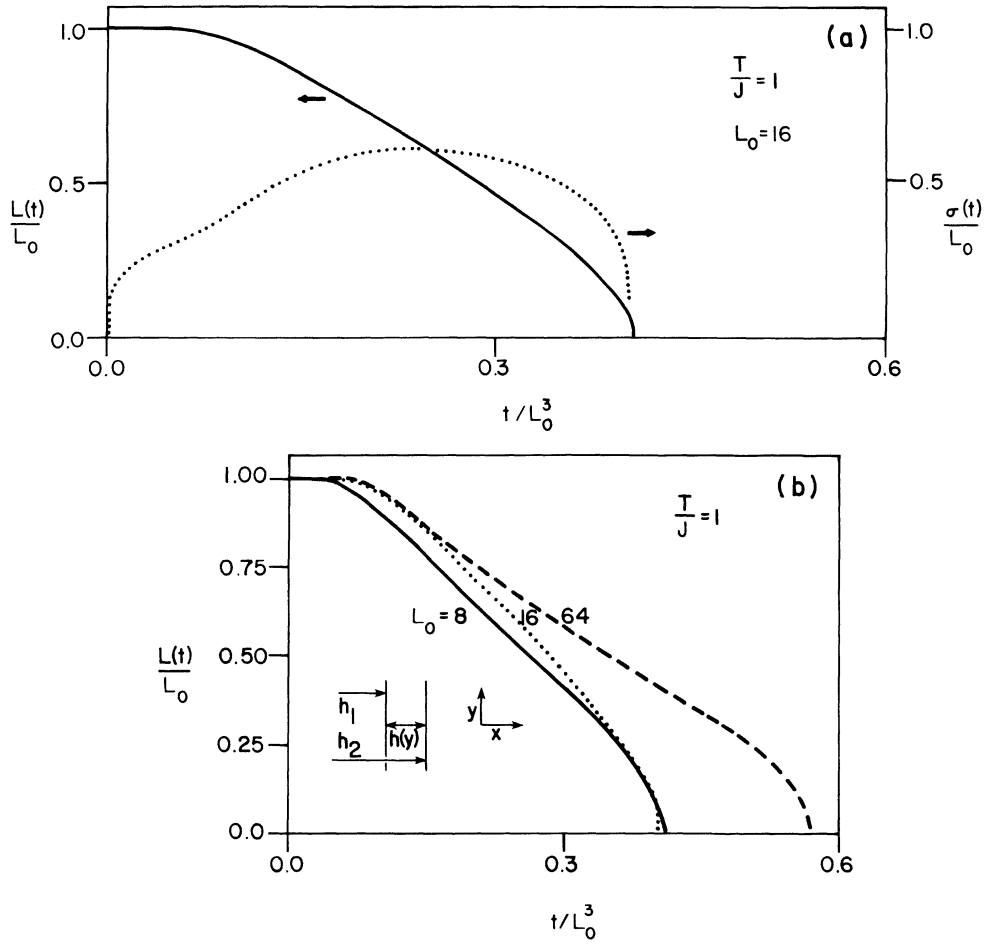

FIG. 4. (a) Width $L(t)$ of an initially strip-shaped domain $[L(0)=L_0]$ is plotted as a function of time using Eq. (33). Also shown is the rms variation $\sigma(t)$ of the average width $L(t)$. The time is normalized to L_0^3 as explained in the text and the temperature in units of the interaction strength J is unity. (b) Domain width $L(t)$ normalized to the initial width L_0 as a function of time for values of $L_0=8$ (solid), 16 (dotted), and 64 (dashed). The inset shows the initial configuration of the two domain walls. The time is normalized to L_0^3 as explained in the text.

A. Strip domain kinetics

The strip geometry considered here is shown in Fig. 4. It consists of an infinite strip of one domain surrounded by semi-infinite planes of the other type of domain. If $h(y,t)$ is the relative separation of the two domain walls, the time development of h is given by the solution of Eq. (22) with the initial condition $h(y,0)=L_0$. If fluctuations are neglected, this equation can be solved for the exponential form for the interaction described above and we find for h in units of $2/\xi$

$$h(y,t)=L_0+\tfrac{1}{2}\ln(1-8J\alpha e^{-2L_0}t)\ . \tag{24}$$

Thus the strip shrinks uniformly and very slowly with a characteristic equilibration time $t\sim\exp(2L_0)$ where L_0 is the initial width. As we shall see, the effects of thermal fluctuations change this characteristic time from being exponentially large in L_0 to a simple power.

To solve the full stochastic equation (22), we make use of a Gaussian ansatz for the time-dependent probability distribution function for the stochastic variable $h(y,t)$. Following Ref. 32, we note that the Langevin equation of motion is equivalent to the Fokker-Planck equation for the probability distribution function P

$$\dot{P}[\{h_i\},t]=\sum_i \frac{\partial}{\partial h_i}\left[\frac{\delta F}{\delta h_i}+2kT\frac{\delta}{\delta h_i}\right]P[\{h_i\},t]\ , \tag{25}$$

where h_i is a spatial discretization of the continuous field $h(y,t)$ and $\delta F/\delta h_i$ are the first two terms of the right-hand side of Eq. (22). The extra factor of 2 comes from the correlation function, Eq. (23). The equations for the first two moments of h_i, its average value $\langle h_i\rangle=L(t)$, and the correlation function $\langle\tilde{h}_i\tilde{h}_j\rangle$ are

$$\dot{L}=-\left\langle\frac{\delta F}{\delta h_i}\right\rangle\ , \tag{26}$$

$$\frac{\partial}{\partial t}\langle\tilde{h}_i\tilde{h}_j\rangle=-\left[\left\langle\tilde{h}_i\frac{\delta F}{\delta h_j}\right\rangle+\left\langle\tilde{h}_j\frac{\delta F}{\delta h_i}\right\rangle\right]$$

$$+4kT\,\delta_{i,j}\ , \tag{27}$$

where $\tilde{h}_i=h_i-L(t)$. Transforming to momentum space we write

$$h_q=\frac{1}{\sqrt{N}}\sum_i h_i e^{-iqy_i}\,, \tag{28a}$$

$$\tilde{h}_q=h_q-\sqrt{N}h_0\delta_{q,0}\,, \tag{28b}$$

$$G(q,t)=\langle\tilde{h}_q\tilde{h}_{-q}\rangle\,, \tag{28c}$$

where N is the number of lattice sites. The probability distribution is parametrized by writing

$$P[\{h_q\},t]\propto\exp\left[-\tfrac{1}{2}\sum_q \tilde{h}_q G^{-1}(q,t)\tilde{h}_{-q}\right]. \tag{29}$$

By properties of the Gaussian, averages such as $\langle e^{iph_i}\rangle$ can easily be performed. Thus

$$\langle e^{i\beta h_i}\rangle=e^{i\beta L(t)}\exp\left[\frac{-\beta^2}{2N}\sum_q G(q,t)\right], \tag{30}$$

$$\left[\frac{\partial}{\partial\delta}\langle e^{i\beta h_i+i\delta\tilde{h}_j}\rangle\right]_{\delta=0}=-\beta e^{i\beta L(t)}\langle\tilde{h}_i\tilde{h}_j\rangle\times\exp\left[\frac{-\beta^2}{2N}\sum_q G(q,t)\right]. \tag{31}$$

Approximating the short-range potential V by a δ function,

$$V(h)=-U_0\delta(h)\,,$$

the equations of motion for the first two moments are

$$\dot{L}=2U_0\left\langle\frac{\partial}{\partial h_i}\delta(h_i)\right\rangle, \tag{32a}$$

$$\frac{\partial}{\partial t}\langle\tilde{h}_i h_j\rangle=\left[J\langle\tilde{h}_i\nabla^2 h_j\rangle+2U_0\left\langle\tilde{h}_i\frac{\partial}{\partial h_j}\delta(h_j)\right\rangle+2kT\,\delta_{i,j}\right]+(i\leftrightarrow j)\,. \tag{32b}$$

Using the Fourier representation of the δ function and Eqs. (30) and (31), we find

$$\dot{L}=-LK^2(t)\,, \tag{33a}$$

$$\dot{G}=2\left\{2kT-G(q,t)\left[Jq^2+K^2\left[1-\frac{L^2}{\sigma^2}\right]\right]\right\}, \tag{33b}$$

$$K^2=2U_0(\sqrt{2\pi}\sigma^3)^{-1}e^{-L^2/2\sigma^2}\,, \tag{33c}$$

$$\sigma^2=\frac{1}{N}\sum_q G(q,t)=\frac{1}{N}\sum_{i=1}^{N}\langle\tilde{h}_i^2\rangle\,. \tag{33d}$$

An analysis of these equations of motion indicates that initially, when the fluctuations are small and $L(t)\ll\sigma$, $\dot{L}(t)\simeq 0$ and σ^2 is proportional to $Tt^{1/2}$. When the fluctuations increase so that $\sigma^2\sim\frac{1}{2}L_0^2$, $L(t)$ begins to decrease. This decrease in the domain width is initially linear in time, with a slope proportional to L_0^{-2}. The characteristic shrinking time scales with L_0^3, much faster than the deterministic result as described above. These results are in agreement with the numerical solutions shown in Fig. 4 where the time dependence of the domain width and mean-square fluctuations are plotted. In Fig. 4(b), the time is scaled by L_0^3 and the initial slopes of the linear regions are the same for all initial L_0. In three dimensions, it would take an exponentially long time for a wall which is initially straight to develop enough fluctuations, since even above the roughening temperature, where the present model is applicable, the initial time dependence of σ is proportional to $T\ln t$.

To test this model which demonstrates how fluctuations greatly increase the kinetics of strip domains in two dimensions, we have carried out Monte Carlo simulations. We have studied the kinetics of strip-shaped domains for both the $p=2$ ferromagnetic Potts model using Glauber dynamics and the Ising antiferromagnetic using Kawasaki dynamics. The domains were taken to be 4, 8, and 12 lattice constants wide and the simulations were performed on rectangular $(N\times M)$ lattices. Although the results obtained from the two different dynamics are in qualitative agreement with each other and show the same scaling

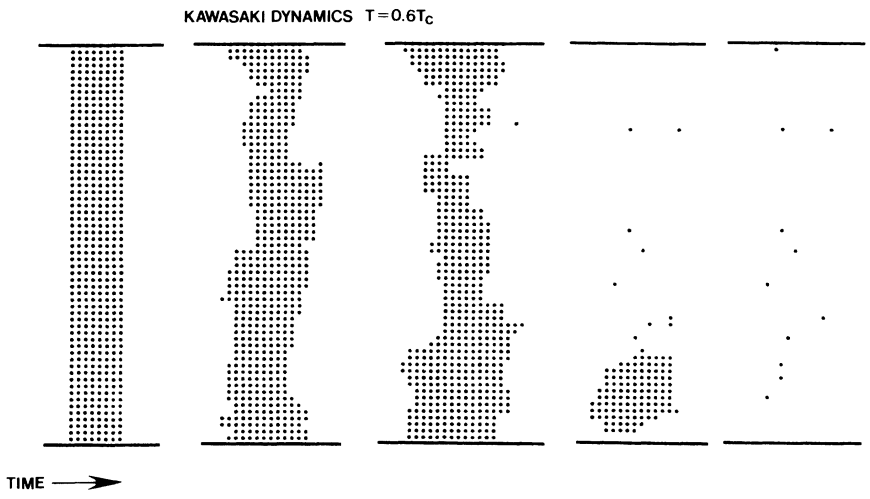

FIG. 5. Evolution of an initially strip-shaped domain for various instants of time for $T=0.6T_c$.

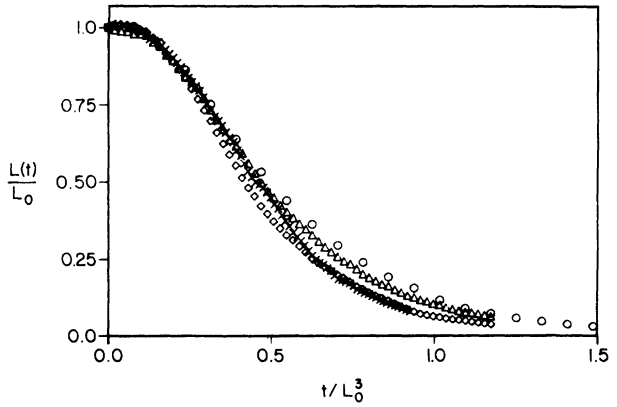

FIG. 6. Normalized domain width $L(t)/L_0$ vs t/L_0 for a strip domain obtained in simulations using Glauber dynamics for $T=0.6T_c$. (a) $L_0=4$, 160×20 lattice (open circles), (b) $L_0=8$, 160×40 lattice (open diamonds), (c) $L_0=8$, 1000×32 lattice (open triangle), and (d) $L_0=12$, 1000×40 lattice (crosses). The data were averaged over 40 runs each for (a) and (b) and over four runs for (c) and (d). Note the agreement with the scaling prediction of the model.

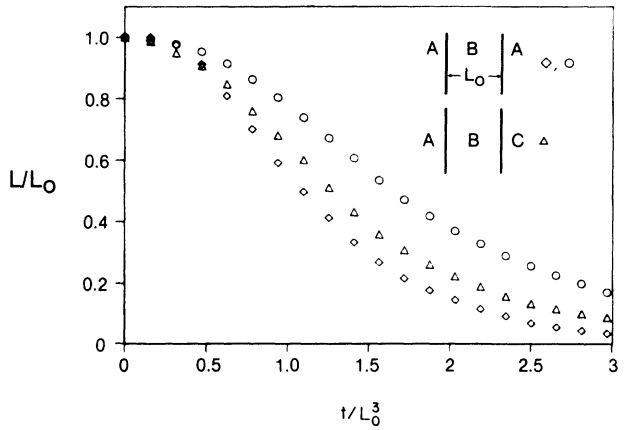

FIG. 8. Normalized domain width $L(t)/L_0$ vs t/L_0^3 for the initial domain configurations shown in the inset. Glauber dynamics were used for $L_0=4$ on a 1000×20 lattice. The circles are for a Potts degeneracy $Q=4$ while the diamonds and triangles are for $Q=3$. The data was averaged over five initial configurations.

behavior, the overall time taken for a strip of a given width to completely disappear is shorter for the spin-flip dynamics as compared with the spin-exchange case.

Diagrams of the shrinking domain are shown in Fig. 5. Data showing the domain width as a function of time are shown in Fig. 6 for Glauber dynamics and in Fig. 7 for Kawasaki dynamics where we plot $L(t)/L_0$ vs t/L_0^3, as suggested by the theoretical results. The time t is in units of Monte Carlo steps per spin and the hopping time is set to unity. The simulations were performed for temperatures $T=0.4T_c$ and $T=0.6T_c$. For an initial short time period which depends on L_0 and T, the average width stays essentially constant, since fluctuations are small and the average curvature is approximately zero. As time increases, fluctuations build up, and the average curvature in some regions along the length of the strip becomes quite large, resulting in the formation of necks where the two domain walls are close. Fluctuations cause these necks to narrow until they finally disappear, leaving the initially long strip divided into a number of ellipses of different sizes. The average curvature of the domains then causes them to shrink rapidly. During this intermediate-time regime, the average width decreases linearly in time with a slope proportional to L_0^{-3} as predicted above. However, for very long times, the average width decreases much slower than linearly in time. This long-time tail is apparently caused by the slow disappearance of some very long domains which are statistically formed in some configurations.

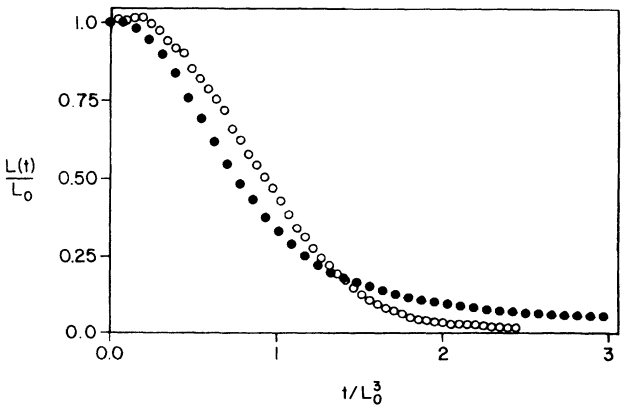

FIG. 7. Normalized domain width $L(t)/L_0$ vs t/L_0^3 using Kawasaki dynamics for $T=0.6T_c$. The open and closed circles correspond to strips of widths $L_0=4$ and 8, respectively, on a rectangular lattice of 1000×32 sites. Again the data scale in agreement with the predictions of the model.

To contrast the dynamics of the strip which are dominated by fluctuations with the dynamics of an interface which is dominated by the deterministic curvature energy, we have also carried out simulations (described below) on an initially circular domain. Here we note that the characteristic time for the disappearance of the circular domain is proportional to the square of the radius while it is proportional to L_0^3 for the strip in two dimensions in the presence of thermal fluctuations and to $\exp(L_0)$ if fluctuations are ignored. These results are in agreement with the predictions of the continuum model for interacting, fluctuating domain walls, as described above. Finally, Fig. 8 shows the time dependence of the width of a strip of one sublattice (Potts spin in B direction) surrounded by half-planes of spins of two different sublattice types (e.g., C on the right and A on the left or A on both sides). For the strip geometry, the results are essentially the same as those of the two component configuration. This is not the case for more complex geometrical arrangements as described in Sec. IV.

B. Circular domain kinetics

In contrast with the strip domain where the kinetics is dominated by fluctuations, an initially circular domain of one spin surrounded by an infinite sea of the other spin shrinks because of the deterministic force due to curva-

ture.[33] However, in contrast to the situation in three dimensions where fluctuations can be ignored, there is a strong temperature dependence to this shrinking rate. We use Eqs. (16) and (17) derived above to describe the kinetics of a nearly circular domain, described by a boundary $R(\theta,t)$. We find that in the absence of the thermal noise term, the area decreases linearly in time, with a temperature-independent coefficient, in agreement with the three-dimensional case that has been previously considered. To analyze the two-dimensional case in the presence of thermal fluctuations, we note that for finite times $R(\theta,t)$ can be calculated by a perturbation theory. This is possible because the roughening of a two-dimensional domain wall is infinite only for infinite times. We thus write

$$R = R_0 + R_1 + R_2 + \cdots \tag{34}$$

with R_0 (the deterministic part) independent of T, and R_1 and R_2 being of order $T^{1/2}$ and T, respectively. In the following, the Boltzman constant is set to unity. Equating equal powers of T in the equations of motion [Eqs. (16) and (17)], we find

$$\dot{R}_0 = -J/R_0 , \tag{35a}$$

$$\dot{R}_1 = JR_1/R_0^2 + JR_{1\theta\theta}/R_0^2 + \eta/R_0^{1/2} , \tag{35b}$$

$$\dot{R}_2 = JR_2/R_0^2 - JR_1^2/R_0^3 + JR_{2\theta\theta}/R_0^2 - 2JR_1R_{1\theta\theta}/R_0^3 - \tfrac{1}{2}\eta R_1/R_0^{3/2} . \tag{35c}$$

The area of the minority domain is then computed as a function of time. Since

$$A = \tfrac{1}{2}\int \langle R^2(\theta)\rangle d\theta \tag{36}$$

only the angle-averaged values of R_0, R_1^2, and R_2 are needed.

To solve these equations, we note that the solution of Eq. (35a) is the deterministic solution

$$R_0^2(0) - R_0^2(t) = 2Jt . \tag{37}$$

The equation for R_1 is linear and may thus be solved by Fourier transformation. We write

$$\langle R_1(0,t)R_1(\theta,t)\rangle = \sum_{n=-N}^{N-1} G_n e^{in\theta} . \tag{38}$$

The cutoff $N=\pi R$ is due to the discreteness of the lattice. Equation (35b) then becomes [see Eq. (25)]

$$\dot{G}_n = 2JG_n(1-n^2)/R_0^2 + T/4\pi R_0 \tag{39}$$

with the solution

$$G_n = \left[\left[\frac{R_0}{L_0} \right]^{2n^2-3} - 1 \right] \frac{1}{(3-2n^2)} \frac{T}{4\pi J} R_0 . \tag{40}$$

The time rate of change of the area is

$$\dot{A} = \pi \frac{\partial}{\partial t} \left[R_0^2 + \sum_n G_n + 2R_0\bar{R}_2 \right] \tag{41}$$

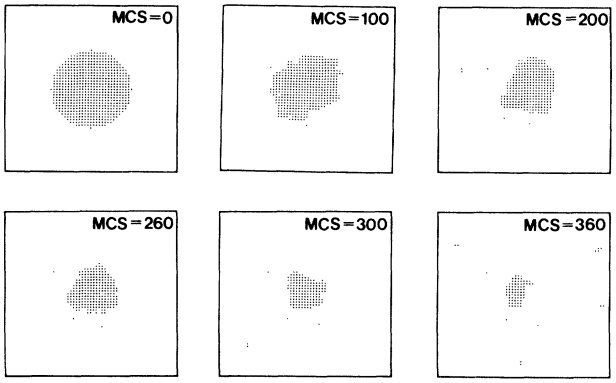

FIG. 9. Evolution of an initially circular domain using Kawasaki dynamics for various instants of time as indicated at the top of each diagram for $T=0.8T_c$.

or

$$\dot{A} = 2\pi \left[-1 + \sum_n \frac{n^2 G_n}{R_0^2} + \frac{T}{8J} \right] \tag{42}$$

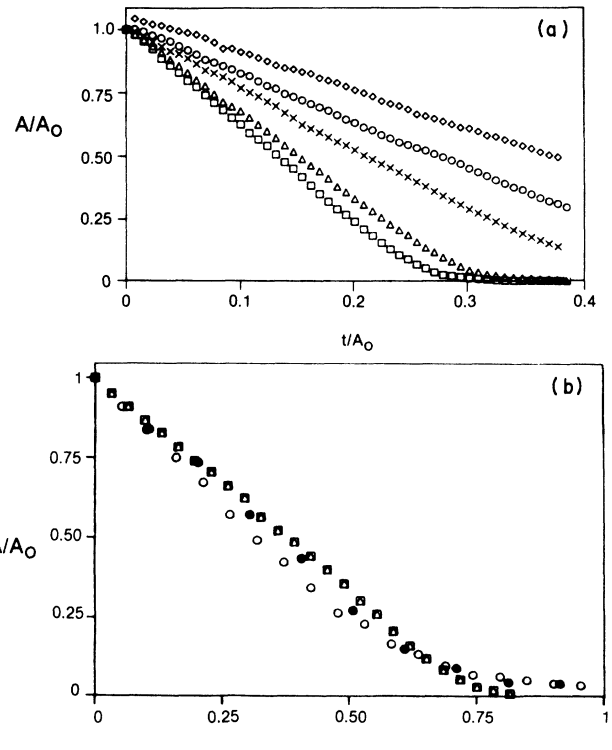

FIG. 10. (a) Normalized area $A(t)/A_0$ vs t/A_0 [$A_0=A(0)$] for circular domains of initial radius $R=20$ lattice constants at different temperatures obtained using Glauber dynamics. The temperature $T=0.9T_c$ (diamonds), $0.8T_c$ (circles), $0.7T_c$ (crosses), $0.5T_c$ (triangles), and $0.4T_c$ (squares). The data were averaged over 60 configurations for $T/T_c=0.9$ and 0.8, 40 configurations for $T/T_c=0.7$ and 0.5, and 20 configurations for $T/T_c=0.4$. The statistical error in A/A_0 is comparable to the size of the symbols. (b) Normalized area $A(t)/A_0$ of an initially circular domain is plotted vs t/A_0 using Kawasaki dynamics. The closed circles, open circles, and squares correspond to circular domains of initial radii of $R_0=8$, 11, and 14 lattice constants, respectively, at $T=0.6T_c$ averaged over 60 configurations.

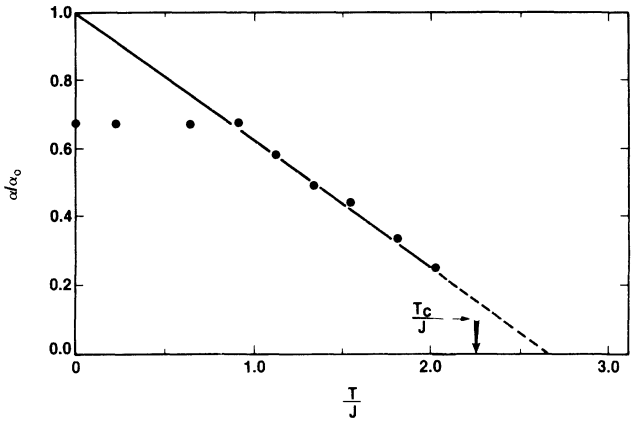

FIG. 11. Shrinking rate $\alpha=\bar{\alpha}/\tau$ [see Eq. (43)] is plotted as a function of temperature normalized to the interaction energy J. The points are the results of Monte Carlo simulations using Glauber dynamics, and the line is the result of the roughening model described in the text. For both the simulations and the model calculation, the hopping time τ has been set to unity. The value for α obtained from the model calculation is normalized to its $T=0$ value.

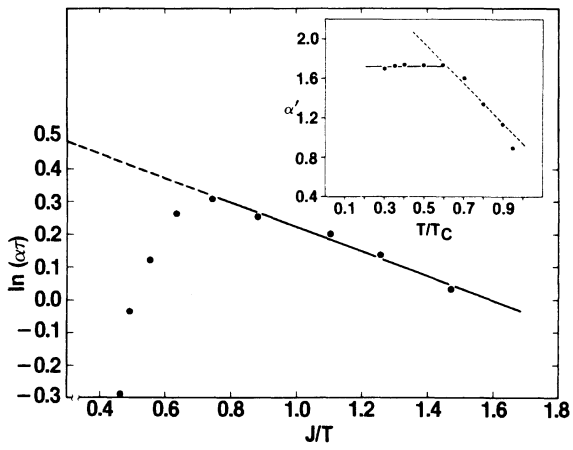

FIG. 12. Logarithm of the slope α obtained from simulations using Kawasaki dynamics is plotted vs J/T. The inset displays $\alpha'=\alpha\tau\exp(0.4J/kT)$ vs T/T_c. Note that α' obtained in this manner has the same temperature dependence as the shrinking rate shown in Fig. 11. At the lowest temperatures, ($T\lesssim 0.3T_c$), α is temperature independent.

with $\bar{R}_2=(1/2\pi)\int_0^{2\pi}R_2 d\theta$. We note that the time is still in units of the hopping time. Using the results for R_0, R_1, and R_2, we find (omitting terms of order $1/R$)

$$\bar{\alpha}\equiv\frac{1}{\pi}\dot{A}\simeq -2\left[1-\frac{3}{8}\frac{T}{J}\right]. \tag{43}$$

Numerical solutions of the equations of motion yield similar results for $\bar{\alpha}$, with some radius-dependent corrections.

The area thus decreases linearly in time, but with a temperature-dependent coefficient which decreases the shrinking rate as the temperature is decreased. We note that this effect is not due to critical fluctuations which are important only for $T\simeq T_c$, but rather to roughening fluctuations of the domain boundary location. The effects of the roughening fluctuations on the kinetics, as seen in the Monte Carlo simulations, are shown in Fig. 9 where diagrams of the evolution of an initially circular domain are shown at different times for $T=0.6T_c$. It is seen that the circular domain roughens very rapidly due to thermal fluctuations. At low temperatures ($T\lesssim 0.5T_c$), we found that the circular domain remained essentially circular throughout its evolution, whereas at $T\gtrsim 0.8T_c$, thermal fluctuations are so strong that the domain becomes extremely wavy in less than ten Monte Carlo steps.

The simulations and the theoretical results can be compared quantitatively as well. Figures 10(a) and 10(b) show the linear time dependence of the area of the domain for several different temperatures. The approximate expression for the shrinking rate $\bar{\alpha}$ is plotted in Fig. 11 along with the results of Monte Carlo simulations for Glauber dynamics for an initial radius of 20 lattice spacings. The analytical results and the simulations have been fit at one point, since the overall time scale used in the simulation differs from that of the continuum theory. In both cases, the hopping time τ has been set to unity; τ could provide some extrinsic, additional temperature dependence in real experimental situations. The agreement between theory and the simulation is excellent in the region $T>J$. In this region $\bar{\alpha}$ is linear in temperature due to the roughening effects. These fluctuations effectively increase the area at any given time, resulting in a decreased $\bar{\alpha}$ when compared with $\bar{\alpha}$ calculated from a deterministic theory. The deviation from the deterministic theory is not small, indicating the importance of these roughening effects.

At low temperature, the simulations show a temperature-independent value which is about 30% lower than that predicted by the extrapolation of the continuum theory to zero temperature (equivalent to the results of Ref. 17). The reason for this discrepancy lies in the effects of the discreteness of both the space lattice and the spins, which do not allow a perfectly circular initial domain. Furthermore, the motion of the domain boundary must proceed in discrete steps in the simulations. Thus when compared with a continuum theory for an initially circular domain, these discreteness effects result in some effective roughness, even at zero temperature. This effective roughness leads to the temperature-independent decrease of $\bar{\alpha}$ at low temperatures from the predicted theoretical values.[34]

The simulations using Kawasaki dynamics yield a more complicated temperature dependence for $\bar{\alpha}$, since the effects of the exchange dynamics introduces another intrinsic temperature dependence for the shrinking rate α. This is shown in Fig. 12 where $\ln(\bar{\alpha})$ vs J/T is plotted. At the lowest temperatures, $\bar{\alpha}$ is temperature independent. For $0.3\lesssim T/T_c\lesssim 0.6$, the Monte Carlo results fall on a straight line with a slope of 0.4. At higher temperatures, however, a strong deviation from linearity (which implies exponential temperature dependence for $\bar{\alpha}$) is found. In the inset of Fig. 11 $\alpha'\equiv\bar{\alpha}e^{0.4J/T}$ is plotted versus T/T_c and a linear decrease (dashed line) of α' is found for $T>0.6T_c$ as above. The deviation at $T=0.95T_c$ from this linear behavior is presumably due to critical fluctuations; the domain walls lose their sharpness at $T\to T_c$. At fixed temperatures ($T=0.8T_c$) we have also observed a weak

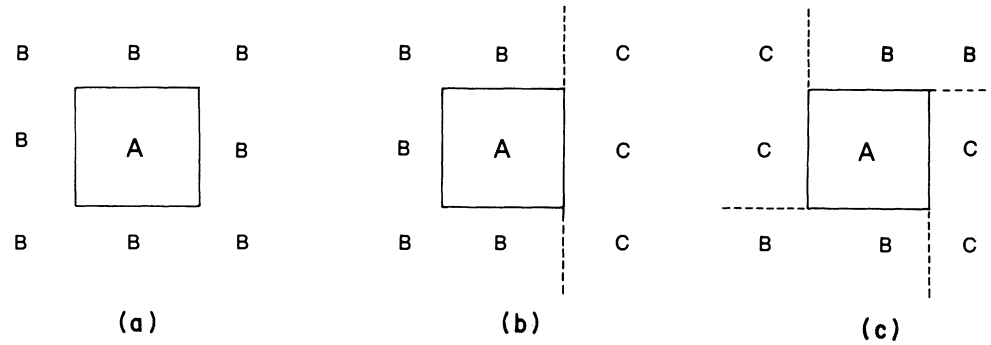

FIG. 13. Three initial configurations used to study the time and temperature dependence of the area $A(t)$ of an initially square domain of Potts spin (sublattice) A surrounded by two other components B and C for the $Q=3$ case.

but systematic dependence of α on the initial radius. As the initial radius is changed from 10 to 20 lattice constants, α increases by $\sim 15\%$. However, as the initial radius is further increased to 33 lattice constants, α decreases by $\sim 20\%$.

Finally, we note that simulations of the kinetics of global quenches[14] on two-component systems have resulted in temperature-dependent growth rates that are identical to those obtained here for the isolated domain studied here. This indicates the utility of our model domain studies where analytic models can be used to understand this temperature dependence in terms of roughening fluctuations of the domain walls. The fact that for the Ising model, the temperature dependence is the same for both the model study and the global quenches reflects the appropriateness of the simple geometry as being a "typically nucleated" domain.

IV. MULTICOMPONENT SYSTEMS: PINNING EFFECTS

In the previous sections we have analyzed the kinetics of a single domain surrounded by an infinite sea of one other type of domain for various geometries and temperatures. In this section, we discuss the kinetics of simple domain geometries for multicomponent ($Q \geq 3$) systems where there is more than one type of domain in the infinite sea and pinning effects drastically change the kinetics.

In Ref. 13, following Lifshitz, we suggested that for a system with at least three degenerate ground states, a hexagonal domain surrounded by alternating sequences of two of the other degenerate states is completely pinned. It was argued that the change in the domain-wall length is zero when the central domain either grows or shrinks if the domain-wall intersections are constrained to lie at 120° angles. Thus if such a domain is nucleated, it will tend to remain in the system, thus preventing equilibration and resulting in an amorphous polycrystalline structure. On a square lattice, the topologically equivalent domain is shown in Fig. 13(c). Again, simple arguments suggest that this domain will neither grow nor shrink at low temperatures.

To confirm this idea we have simulated a topologically similar initial domain of one superlattice (e.g., type A) in a square geometry as shown in Fig. 13(c). For the domains labeled (a) and (b), the curvature energy is the driving force for shrinking. These domains indeed shrink with an

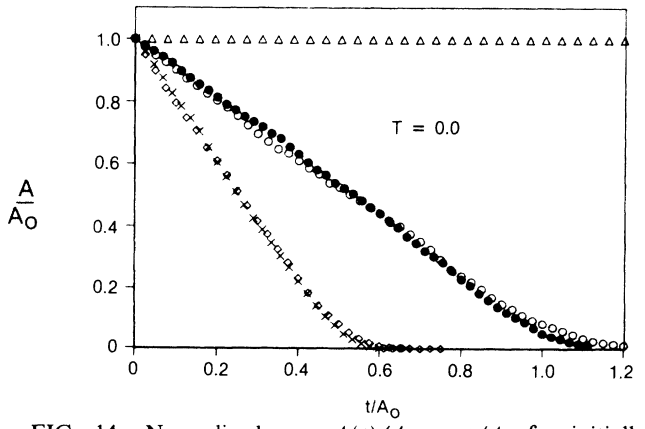

FIG. 14. Normalized area $A(t)/A_0$ vs t/A_0 for initially square domains of Potts spin A surrounded by the three configurations of spins B and C shown in Fig. 13. The simulations were carried out using Glauber dynamics for a $Q=3$ model at zero temperature. For configuration (a) of Fig. 13, the diamonds and crosses are for $A_0=400$ and 900, respectively, where the length scale is the lattice constant. The open ($A_0=400$) and closed ($A_0=900$) circles are for initial configurations (b) and the open triangles are for configuration (c) for any A_0. The time t is measured in units of the hopping time τ. The data were averaged over 20 initial configurations.

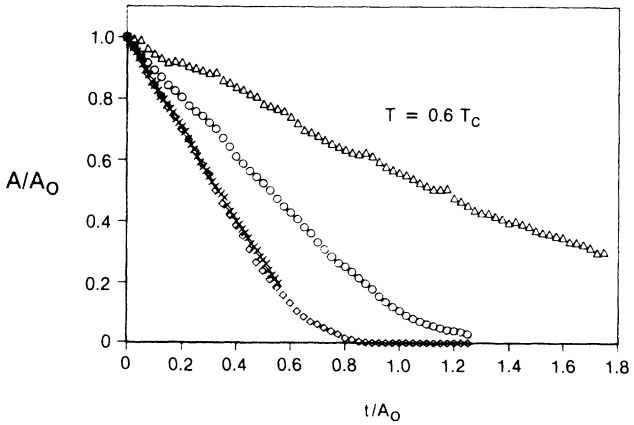

FIG. 15. Normalized area $A(t)/A_0$ vs t/A_0 for initially square domains shown in Fig. 13. The simulations were carried out using Glauber dynamics for a $Q=3$ model at $T=0.6T_c$. The symbols are the same as used in Fig. 14. Note that configuration (c) of Fig. 13 (open triangles, $A_0=400$) now collapses due to roughening fluctuations. The data were averaged over 20 configurations.

area that decreases linearly in time, as for the circular geometry discussed above. Figure 14 contrasts the zero-temperature kinetics of these domain geometries with that of the pinned geometry [Fig. 13(c)] which is pinned at $T=0$ since we only use single spin-flip dynamics. This result is in agreement with the prediction based upon the assumption of fixed angles between intersecting domain walls. In the present example on the square lattice, this angle is either 90° or 180°. Given this constraint, the total wall length in Fig. 13(c) remains the same if the central domain (A) either grows or shrinks, leading to the observed pinning.

At high temperatures, thermal fluctuations, which roughen the domain walls, speed up the kinetics of this slowly equilibrating domain. This is shown in Fig. 15 where the area is plotted as a function of time for $T=0.6T_c$. The domain which was pinned at zero temperature is now shrinking. The physical origin of the increased kinetics lies in the roughening fluctuations which are similarly responsible for the kinetics of the strip-shaped domain as discussed in Sec. III A. The large fluctuations between samples observed in this simulation make it difficult to determine whether the exponent for the shrinking rate for case (c) is different than the linear rate observed for the circlelike domains in (a) and (b) of Fig. 13.

In the following paper, similar kinetics are observed in global quenches of multicomponent systems on square lattices. It is shown that the domain geometry of Fig. 13(c) is typically nucleated and is responsible for the extremely slow kinetics observed in the simulations at low temperatures. At higher temperatures, roughening fluctuations speed up the equilibration of the global quenched system. However, on the triangular lattice, the hexagonal domains discussed in Ref. 13 are not nucleated and the system is thus not pinned, even at low temperatures. These comparisons indicate the utility of studying the model domain geometries analyzed in this paper, since their kinetics can be simply understood in terms of both pinning and roughening. The global quenches can be understood in terms of the kinetics of the typically nucleated domain geometries. This will be examined further in the following paper.

ACKNOWLEDGMENT

The authors acknowledge useful discussions with B. White and D. Srolovitz.

[1]For a general review, see *Ordering in Two Dimensions*, edited by S. K. Sinha (Plenum, New York, 1980).
[2]P. M. Horn, R. J. Birgeneau, P. Heiney, and E. M. Hammonds, Phys. Rev. Lett. 41, 961 (1978).
[3]P. W. Stephens, P. Heiney, R. J. Birgeneau, and P. M. Horn, Phys. Rev. Lett. 43, 47 (1979); W. C. Marra, P. H. Puoss, and P. E. Eisenberger, *ibid.* 49, 1169 (1982).
[4]J. C. Bucholz and M. G. Lagally, Phys. Rev. Lett. 35, 442 (1975); T. M. Lu, G. C. Wang, and M. G. Lagally, *ibid.* 39, 411 (1977).
[5]L. D. Roelofs, T. L. Einstein, and M. G. Lagally, Phys. Rev. Lett. 39, 411 (1977); M. G. Lagally, G. C. Wang, and T. M. Lu, CRC Crit. Rev. Solid State Mater. Sci. 7, 233 (1978).
[6]T. J. Estrup, in *Ordering in Two Dimensions*, Ref. 1, M. K. Debe and D. A. King, Surf. Sci. 81, 193 (1979).
[7]See *Physics of Intercalation Compounds*, edited by L. Pietronero and E. Tossatti (Springer, New York, 1981), Part IV.
[8]J. R. Banavar, G. S. Grest, and D. Jasnow, Phys. Rev. Lett. 45, 1424 (1980).
[9]P. S. Sahni and J. D. Gunton, Phys. Rev. Lett. 47, 1754 (1981).
[10]J. W. Sacco and J. Chalupa, Solid State Commun. 39, 75 (1981); O. G. Mouristen and A. J. Berlinsky, Phys. Rev. Lett. 48, 181 (1982).
[11]P. S. Sahni, G. S. Grest, M. P. Anderson, and D. J. Srolovitz, Phys. Rev. Lett. 50, 263 (1983).
[12]I. M. Lifshitz, Zh. Eksp. Teor. Fiz. 42, 1354 (1972) [Sov. Phys.—JETP 15, 939 (1962)].
[13]S. A. Safran, Phys. Rev. Lett. 46, 1581 (1981).
[14]P. S. Sahni, D. J. Srolovitz, G. S. Grest, M. P. Anderson, and S. A. Safran, following paper, Phys. Rev. B 28, 2705 (1983).
[15]S. T. Chui and J. D. Weeks, Phys. Rev. Lett. 40, 733 (1978).
[16]J. S. Langer, Ann. Phys. (N.Y.) 65, 53 (1971).
[17]S. M. Allen and J. W. Cahn, Acta Metall. 27, 1085 (1979).
[18]A. T. English, Trans. Metall. Soc. AIME 236, 14 (1966).
[19]S. A. Safran, P. S. Sahni, and G. S. Grest, Phys. Rev. B 26, 466 (1982).
[20]G. S. Grest, S. A. Safran, and P. S. Sahni, J. Magn. Magn. Mater. 31-34, 1011 (1983).
[21]P. S. Sahni and G. S. Grest, J. Appl. Phys. 53, 8002 (1982).
[22]P. S. Sahni, G. S. Grest, and S. A. Safran, Phys. Rev. Lett. 50, 60 (1983).
[23]A. N. Berker, S. Ostlund, and F. A. Putnam, Phys. Rev. B 17, 3650 (1978).
[24]S. Alexander, Solid State Commun. 14, 1069 (1974).
[25]*Monte Carlo Methods in Statistical Physics*, edited by K. Binder (Springer, Berlin, 1979).
[26]P. C. Hohenberg and B. I. Halperin, Rev. Mod. Phys. 49, 435 (1977).
[27]J. S. Langer, M. Bar-on, and H. D. Miller, Phys. Rev. A 11, 1417 (1975); C. Billotet and K. Binder, Z. Phys. B 32, 195 (1979).
[28]K. Kawasaki and T. Ohta, Proceedings of Conference on Nonlinear Fluid Behavior, Boulder, Colorado, 1982 (in press); Prog. Theor. Phys. 62, 147 (1982).
[29]G. F. Mazenko, Phys. Rev. B 26, 5103 (1982); G. F. Mazenko and O. T. Valls *ibid.* 27, 6811 (1983).
[30]G. F. Mazenko and P. S. Sahni, Phys. Rev. B 18, 6139 (1978); P. S. Sahni and G. F. Mazenko, *ibid.* 20, 4674 (1979).
[31]P. Bak, in *Solitons and Condensed Matter Physics*, edited by A. T. Bishop and T. Schneider (Springer, New York, 1978), p. 216.
[32]Y. Saito, Z. Phys. B 32, 75 (1978).
[33]P. S. Sahni, G. Dee, J. D. Gunton, P. Phani, J. L. Lebowitz, and M. Kalos, Phys. Rev. B 24, 410 (1981).
[34]To rule out the effects of initial domain size on the low-temperature behavior of α, we have performed simulations using Glauber dynamics for initial radii of 20, 30, and 36 lattice constants. At $T=0$, all these initial conditions result in the same value of α.